Nonadiabatic geometric quantum gates that are robust against systematic errors

Yan Liang,[1,2,*,‡] Yi-Xuan Wu,[2,‡] and Zheng-Yuan Xue[2,3,†]

[1] *School of Physical Science and Technology, Guangxi Normal University, Guilin 541004, China*

[2] *Key Laboratory of Atomic and Subatomic Structure and Quantum Control (Ministry of Education), Guangdong Basic Research Center of Excellence for Structure and Fundamental Interactions of Matter, and School of Physics, South China Normal University, Guangzhou 510006, China*

[3] *Guangdong Provincial Key Laboratory of Quantum Engineering and Quantum Materials, Guangdong-Hong Kong Joint Laboratory of Quantum Matter, and Frontier Research Institute for Physics, South China Normal University, Guangzhou 510006, China*

(Received 21 March 2024; revised 18 June 2024; accepted 7 August 2024; published 23 August 2024)

A nonadiabatic geometric quantum gate is realized by integrating nonadiabatic geometric phases with global geometric features into the unitary quantum control, thereby removing the limitation of a long evolution time in the adiabatic case. However, systematic errors are inevitable in practical quantum control; these lead to the deviation of the evolution from target conditions to inducing geometric phases, smearing the robustness of the induced geometric quantum gates. Here, we present a general theoretical framework with enhanced robustness for geometric quantum gates by preserving fundamental geometric conditions. We first analytically evaluate the influence of systematic errors on geometric gates and then propose an optimized approach to mitigate this influence. Numerical simulations indicate that, as the geometric conditions are still maintained in the presence of systematic errors in our scheme, the constructed geometric quantum gates exhibit strong robustness, far superior to that of conventional schemes. Furthermore, we propose implementing the scheme in superconducting quantum circuits, where geometric quantum gates can achieve high fidelity with current experimental parameters. Therefore, the enhanced gate performance highlights the promise of our scheme for large-scale quantum computations.

DOI: 10.1103/PhysRevApplied.22.024061

I. INTRODUCTION

Quantum computation has enormous potential applications and can handle certain problems that are hard for classical computers [1]. Reliable quantum information processing requires the ability to implement high-fidelity quantum gates. However, environmental-induced decoherence and inevitable control errors in quantum manipulation will degrade the gate fidelity. Geometric phases, both abelian [2,3] and non-abelian [4,5], due to their global geometric nature, exhibit inherent resistance to certain local noise [6–8], making geometric quantum computation a promising strategy to enhance the robustness of quantum gates.

Early approaches to geometric quantum computation [9,10] employed adiabatic evolution to suppress transitions between instantaneous eigenstates of the Hamiltonian. However, the adiabatic condition results in prolonged gate operation times, reducing gate performance due to decoherence. To address this constraint, nonadiabatic geometric quantum computation (NGQC) [11,12] and nonadiabatic holonomic quantum computation (NHQC) [13,14] based on abelian and non-abelian geometric phases were introduced. The combination of control robustness and rapid operations has expedited the theoretical development [15–35] and stimulated experimental validations in various physical systems [36–47].

However, NGQC and NHQC schemes necessitate strict adherence to geometric conditions, namely, the cyclic evolution condition and parallel-transport condition, imposing stringent requirements on the driving Hamiltonian. In the presence of systematic errors, defects in these conditions are induced, leading to nonclosed evolution paths and nonzero dynamical phases [48], thereby diminishing the robustness of geometric phases. There are many proposals to enhance the robustness of NGQC and NHQC, such as optimal control [49–51], composite pulse [22,52,53], and optimization algorithms [54], but the fundamental problem of geometric condition defects induced by systematic errors remains unresolved.

Here, different from previous works, we present a general theoretical framework with enhanced robustness for geometric quantum gates by preserving fundamental

*Contact author: liangyan9009@163.com

†Contact author: zyxue83@163.com

‡Y. Liang and Y.-X. Wu contributed equally to this work.

geometric conditions. We first analyze the influence of systematic errors on cyclic evolution and parallel-transport conditions, as well as the induced gate infidelity. Subsequently, we introduce an optimized NGQC (ONGQC) scheme. In the presence of systematic errors, our scheme can maximize the preservation of cyclic evolution and parallel-transport conditions that are essential for NGQC, by optimizing the path parameters. Numerical simulations demonstrate the remarkable performance of our scheme against systematic errors, surpassing both conventional NGQC and dynamical (DY) schemes, as well as previous optimization approaches. In addition, we further propose implementing this scheme in superconducting quantum circuits, where high-performance geometric quantum gates can be achieved with current technologies. Our scheme is readily implementable, and thus, is promising for future large-scale quantum computation.

II. THE OPTIMIZED NGQC

In this section, we first present how to construct the nonadiabatic geometric quantum gate by reverse engineering of the Hamiltonian in a two-level quantum system. Second, we analytically evaluate the influence of systematic errors on geometric gates. Finally, we propose an optimized approach to mitigate the influence of systematic errors on target geometric quantum gates.

A. Inverse engineering of NGQC

We first proceed to construct the nonadiabatic geometric quantum gate by reverse engineering of the target Hamiltonian. Consider a two-level system with lower and upper energy levels denoted by $|0\rangle$ and $|1\rangle$: assuming $\hbar = 1$ hereafter, in the interaction picture, the Hamiltonian for a resonantly driven two-level system can be written as

$$H(t) = \begin{pmatrix} 0 & \Omega_R(t) - i\Omega_I(t) \\ \Omega_R(t) + i\Omega_I(t) & 0 \end{pmatrix}, \quad (1)$$

where the specific forms of $\Omega_R(t)$ and $\Omega_I(t)$ are yet to be determined, and they represent the real and imaginary components of the Rabi frequency. A set of orthogonal solutions of the time-dependent Schrödinger equation, $i|\dot{\psi}_\pm(t)\rangle = H(t)|\psi_\pm(t)\rangle$, can be constructed as

$$\begin{aligned} |\psi_+(t)\rangle &= e^{-if(t)/2}|\phi_+(t)\rangle, \\ |\psi_-(t)\rangle &= e^{if(t)/2}|\phi_-(t)\rangle, \end{aligned} \quad (2)$$

with

$$\begin{aligned} |\phi_+(t)\rangle &= \cos\frac{\theta(t)}{2}e^{-i\alpha(t)/2}|0\rangle + \sin\frac{\theta(t)}{2}e^{i\alpha(t)/2}|1\rangle, \\ |\phi_-(t)\rangle &= \sin\frac{\theta(t)}{2}e^{-i\alpha(t)/2}|0\rangle - \cos\frac{\theta(t)}{2}e^{i\alpha(t)/2}|1\rangle, \end{aligned} \quad (3)$$

where parameters $\theta(t)$ and $\alpha(t)$ denote the time-dependent polar and azimuth angles on a Bloch sphere, respectively, and $f(t)$ is the global phase with $f(0) = 0$. Thus, the path of evolution states, $|\psi_\pm(t)\rangle$, can be visualized on the Bloch sphere.

Furthermore, utilizing the reverse engineering of the target Hamiltonian [24,55–57], i.e., $H(t) = i\sum_{j=\pm}|\dot{\psi}(t)\rangle_j\langle\psi(t)|$, the parameters in Eq. (1) can be determined as

$$\begin{aligned} \Omega_R &= \frac{1}{2}(\dot{f}\cos\alpha\sin\theta - \dot{\theta}\sin\alpha), \\ \Omega_I &= \frac{1}{2}(\dot{f}\sin\alpha\sin\theta + \dot{\theta}\cos\alpha), \end{aligned} \quad (4)$$

where the condition of $\dot{\alpha} = -\dot{f}\cos\theta$ is used to ensure that driving is resonant. Additionally, when the cyclic evolution condition is satisfied at the final time τ, i.e., $|\phi_\pm(\tau)\rangle = |\phi_\pm(0)\rangle = |\psi_\pm(0)\rangle$, the corresponding evolution operator is

$$U(\tau) = \sum_{j=\pm} e^{\mp if(\tau)/2}|\psi_j(0)\rangle\langle\psi_j(0)|. \quad (5)$$

During the process, the overall phase, $f(\tau)$, has both geometric and dynamical components, with the dynamical phase being calculated as

$$\gamma_d(\tau) = \int_0^\tau \langle\phi_+(t)|H(t)|\phi_+(t)\rangle dt = -\int_0^\tau \frac{\dot{\alpha}\sin^2\theta}{2\cos\theta}dt. \quad (6)$$

To induce a pure geometric phase, the dynamical phase should be zero at the end of the cyclic evolution, i.e., $\gamma_d(\tau) = 0$. To this end, the conventional NGQC schemes [21,22] set time-independent azimuth angles, that is, $\dot{\alpha} = 0$, and the corresponding path of the evolution state, $|\psi_+(t)\rangle$, is a closed path passing through the north and south poles, as shown in the left side of Fig. 1(a).

B. Robust conditions for NGQC

However, regarding robustness against systematic errors, the conventional NGQC scheme lacks sufficient advantages over the standard DY scheme in most cases. In the following, we examine the influence of systematic errors on quantum evolution. The Hamiltonian becomes $H'(t) = H(t) + V(t)$, where the error term is

$$V(t) = \begin{pmatrix} \eta\Omega_m & \epsilon(\Omega_R - i\Omega_I) \\ \epsilon(\Omega_R + i\Omega_I) & -\eta\Omega_m \end{pmatrix}, \quad (7)$$

with Ω_m being the maximum pulse amplitude; ϵ and η are the error fractions of Rabi error and the frequency-shift

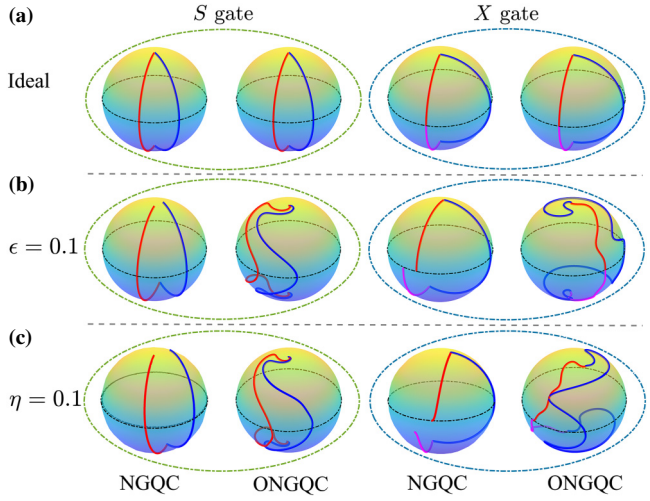

FIG. 1. Schematic illustration of the evolution paths for S and X gates. (a) Evolution paths of both the NGQC and our ONGQC schemes in the absence of errors, where the ONGQC scheme does not require optimization in this case ($c_n = 0$). In the presence of (b) Rabi error with $\epsilon = 0.1$ and (c) frequency-shift error with $\eta = 0.1$, evolution paths of the NGQC scheme deviate from closed path, whereas evolution paths of the ONGQC scheme are still closed paths.

error, respectively. The evolution operator with errors is

$$U'(\tau) = \sum_{j=\pm} |\psi_j'(\tau)\rangle\langle\psi_j(0)|, \tag{8}$$

where $|\psi_j'(\tau)\rangle$ denote the evolution states, which satisfy the Schrödinger equation, $i|\dot{\psi}'(t)\rangle = H'(t)|\psi'(t)\rangle$.

An important condition for realizing a NGQC gate is cyclic evolution, that is, $|\psi_\pm(\tau)\rangle = e^{\mp i f(\tau)/2}|\psi_\pm(0)$. Nevertheless, errors introduce deviations, $\langle\psi_j'(\tau)|\psi_j(\tau)\rangle \neq 1$, disrupting the cyclic condition. Intuitively, errors lead to nonclosed evolution paths on the Bloch sphere in a conventional NGQC, as depicted in Figs. 1(b) and 1(c). Another vital condition for NGQC gates is the parallel-transport condition, $\gamma_d(\tau) = 0$. However, errors induce a nonzero dynamical phase, as illustrated in Figs. 2(a) and 2(c). Violation of these conditions diminishes the robustness of conventional NGQC gates against systematic errors, lacking sufficient advantages compared to standard dynamical gates, as demonstrated in Figs. 3 and 4. Hence, ensuring the conditions of cyclic evolution and zero dynamical phase under systematic errors is crucial for the immunity of geometric quantum gates.

Now we analytically derive the conditions for cyclic evolution to be satisfied in the presence of errors. Defining

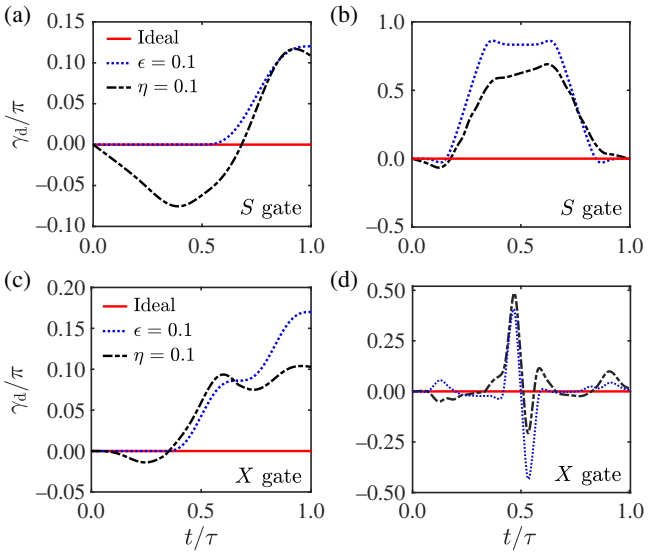

FIG. 2. Dynamical phase $\gamma_d(t)$ for S and X gates: (a),(c) NGQC schemes; (b),(d) ONGQC schemes.

the gate fidelity as [58]

$$\begin{aligned} F &= \frac{1}{2}|\mathrm{Tr}(U^\dagger(\tau)U'(\tau))|, \\ &= \frac{1}{2}[\langle\psi_+'(\tau)|\psi_+(\tau)\rangle + \langle\psi_-'(\tau)|\psi_-(\tau)\rangle], \end{aligned} \tag{9}$$

in the absence of errors, the cyclic condition holds, i.e., $|\psi_\pm'(\tau)\rangle = |\psi_\pm(\tau)\rangle = e^{\mp i f(\tau)/2}|\psi\pm(0)$, and $F = 1$. In the presence of errors, the fidelity is expanded to the second-order perturbation, resulting in (see Appendix C for details):

$$F = 1 - \mathcal{E}^\epsilon - \mathcal{E}^\eta, \tag{10}$$

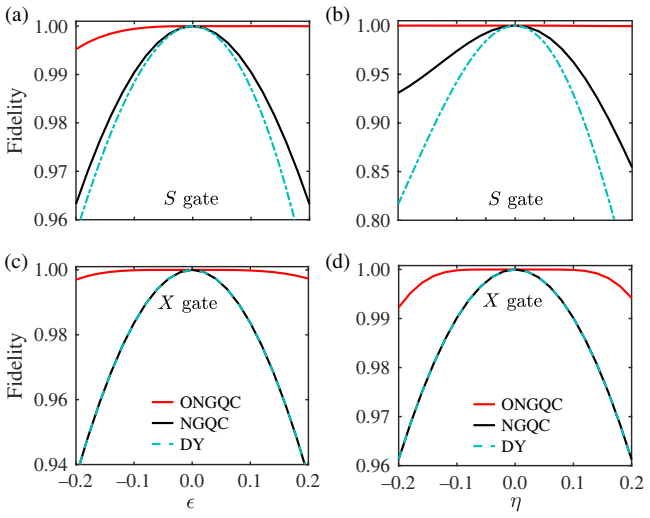

FIG. 3. Gate fidelities as a function of ϵ for (a) S gate and (c) X gate, and as a function of η for (b) S gate and (d) X gate.

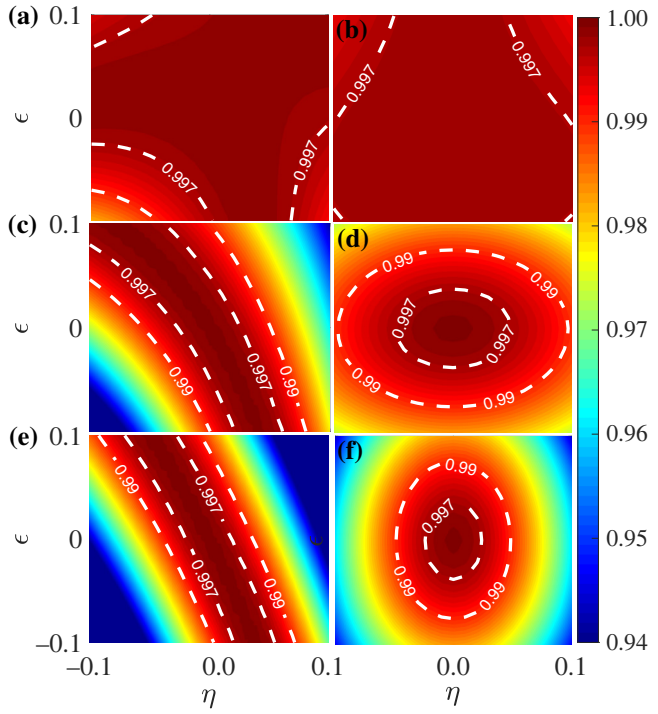

FIG. 4. For a decoherence rate of $\Gamma = 10^{-4}\Omega_m$, the comprehensive performance of the S gate in (a) ONGQC, (c) NGQC, and (e) DY schemes, and the comprehensive performance of the X gate in (b) ONGQC, (d) NGQC, and (f) DY schemes.

where

$$\mathcal{E}^{\epsilon} = \frac{1}{8}\left(\left|\int_0^{\tau} \epsilon \dot{f}\sin^2\theta \,\mathrm{d}t\right|^2 + \left|\int_0^{\tau} \epsilon\left(\frac{1}{2}\dot{f}\sin 2\theta - i\dot{\theta}\right)e^{if}\,\mathrm{d}t\right|^2\right), \tag{11a}$$

$$\mathcal{E}^{\eta} = \frac{1}{8}\left(\left|\int_0^{\tau} \eta\Omega_m \cos\theta \,\mathrm{d}t\right|^2 + \left|\int_0^{\tau} \eta\Omega_m \sin\theta e^{if}\,\mathrm{d}t\right|^2\right), \tag{11b}$$

which denote the adverse influence of the Rabi error and frequency-shift error, respectively, on cyclic evolution. Therefore, to maintain the robustness of geometric quantum gates against systematic errors, we need to minimize the error-influence terms, $\mathcal{E}^{\epsilon}$ and $\mathcal{E}^{\eta}$, as well as the dynamical phase:

$$\gamma_d = \int_0^{\tau} \langle\psi'_+(t)|H'(t)|\psi'_+(t)\rangle \mathrm{d}t. \tag{12}$$

Note that when systematic error fractions ϵ and η are time independent or vary slowly enough during a gate operation, Eq. (11) is valid. However, if ϵ and η vary rapidly and unpredictably, minimizing Eq. (11) becomes impractical, thus impeding the effectiveness of our method.

C. Optimal control

We now propose an ONGQC to minimize the error-influence terms and the dynamical phase by optimizing path parameters. We express f as a function of θ and expand it into a Fourier series of

$$f(\theta) = \sum_{n=1}^{N} c_n \sin 2n\theta, \tag{13}$$

where c_n is a free real parameter. Following the conventional NGQC schemes [21,22,25,48], we divide the evolution path into three segments. In each segment, the polar angle, $\theta(t)$, satisfies boundary conditions $\theta(0) = \theta_0, \theta(\tau_1) = 0, \theta(\tau_2) = \pi, \theta(\tau) = \theta_0$. And the azimuth angles, $\alpha(t)$, satisfy the boundary conditions

$$\begin{aligned} &\alpha(0) = \alpha_0, \alpha(\tau_1) = \alpha_0 + \textstyle\int_0^{\tau_1} \dot{\alpha}\mathrm{d}t, && t \in [0, \tau_1], \\ &\alpha(\tau_1) = \alpha(\tau_1) + \gamma_g, \alpha(\tau_2) = \alpha(\tau_1) + \textstyle\int_{\tau_1}^{\tau_2} \dot{\alpha}\mathrm{d}t, && t \in [\tau_1, \tau_2], \\ &\alpha(\tau_2) = \alpha(\tau_2) - \gamma_g, \alpha(\tau) = \alpha_0, && t \in [\tau_2, \tau], \end{aligned} \tag{14}$$

which include a sudden change in azimuth angles, $\alpha(t)$, at the north and south poles of the Bloch sphere. This is consistent with conventional NGQC schemes; see Appendix A for details. To ensure a smooth pulse, $\theta(t)$ needs to satisfy $\dot{\theta}(0) = \dot{\theta}(\tau_1) = \dot{\theta}(\tau_2) = \dot{\theta}(\tau) = 0$. Then, we optimize the parameter c_n to minimize its adverse influence on cyclic evolution and dynamical phases in Eqs. (11) and (12).

To clarify the optimization process, we consider the S and X gates as examples, with $(\theta_0, \alpha_0, \gamma_g)$ set to $(0, 0, \pi/4)$ and $(\pi/2, 0, \pi/2)$, respectively. For the S gate, requiring only two segments due to $\theta(0) = 0$, we can choose $\theta(t) = \pi\sin^2(\pi t/2\tau_1)$ and $\tau_1 = \tau/2$ to satisfy the boundary conditions. For the X gate, we set

$$\theta(t) = \begin{cases} \dfrac{\pi}{2} - \dfrac{\pi}{2}\sin^2\dfrac{\pi t}{2T_a}, & t \in [0, \tau_1], \\ \pi\sin^2\dfrac{\pi(t-\tau_1)}{2T_b}, & t \in [\tau_1, \tau_2], \\ \pi - \dfrac{\pi}{2}\sin^2\dfrac{\pi(t-\tau_2)}{2T_c}, & t \in [\tau_2, \tau], \end{cases} \tag{15}$$

where $T_a = \tau_1$, $T_b = \tau_2 - \tau_1$, and $T_c = \tau - \tau_2$.

We numerically minimize Eqs. (11) and (12), with c_n as variables. This process involves initializing with an initial guess of c_n and then determining the optimal parameters that minimize the objective functions. Through the optimization of parameter c_n, we minimize Eqs. (11) and (12), ensuring the satisfaction of the cyclic condition in the presence of various types of errors, while maintaining the dynamical phase close to zero. Table I presents the optimized values of parameter c_n for the S gate and the X gate under various types of error. In addition, here we truncate with $n = 5$, which is arbitrary, but this setting is

TABLE I. Optimization parameters c_n for different types of errors. Case 1 addresses the Rabi error; case 2 addresses the frequency-shift errors; and case 3 includes both the Rabi error and frequency-shift errors, as well as decoherence.

		Segment I					Segment II					Segment III				
Case	Gate	c_1	c_2	c_3	c_4	c_5	c_1	c_2	c_3	c_4	c_5	c_1	c_2	c_3	c_4	c_5
1	S	2.89	1.05	0.24	0.01	0.01	2.89	1.05	0.24	0.01	−0.01	...	...	...	...	...
	X	−0.13	−0.49	−0.25	−0.05	−0.09	0	−3.1	−1.22	−0.35	−0.18	0.12	0.32	0.2	0.22	0.03
2	S	2.51	1.22	0.54	0.18	0.10	2.51	1.22	0.54	0.18	0.10	...	...	...	...	...
	X	0.03	0.43	0.36	0.25	0.19	0.11	−2.42	−0.31	0.1	−0.08	0.19	0.56	−0.03	0.13	0
3	S	2.41	1.22	0.54	0.18	0.04	2.41	1.22	0.54	0.18	0.04	...	...	...	...	...
	X	−0.13	−0.49	−0.25	−0.05	−0.09	−0.01	−2.91	−1.22	−0.36	−0.19	0.12	0.32	0.2	0.22	0.03

accurate enough for our purpose. Figure 1 illustrates the evolution paths of our ONGQC and conventional NGQC schemes. In the absence of errors, the ONGQC scheme, without optimization ($c_n = 0$), exhibits a closed path along the longitude for both the ONGQC and NGQC schemes. However, in the presence of Rabi or frequency-shift errors, the evolution path of the NGQC scheme no longer remains closed, while the ONGQC scheme maintains closure, as shown in Figs. 1(b) and 1(c). These facts illustrate that, by minimizing Eq. (11) through parameter optimization, the cyclic condition can be satisfied. Additionally, by minimizing Eq. (12), the ONGQC scheme achieves a near-zero dynamical phase, as shown in Figs. 2(b) and 2(d), i.e., the obtained phase is almost purely geometric, and thus, promises a good gate performance. Conversely, errors cause the conventional NGQC scheme to have a large nonzero dynamical phase, as shown in Figs. 2(a) and 2(c), which leads to poor gate performance under these systematic errors.

Through parameter optimization, the fundamental conditions of NGQC, i.e., cyclic evolution and zero dynamical phase, are well satisfied, significantly enhancing the robustness of the implemented geometric quantum gates against systematic errors. In Fig. 3, we demonstrate the numerical results for the robustness of the S gate and X gate in the ONGQC scheme against Rabi errors (case 1) and frequency-shift errors (case 2), and compare them with both the conventional NGQC scheme and the DY scheme; see Appendixes A and B for their respective implementation details. These results show that our scheme exhibits exceptional immunity to systematic errors, maintaining a fidelity above 99% across the entire range of systematic errors.

To assess the experimental relevance of the ONGQC scheme, we numerically simulate the comprehensive performance of the quantum gate using the master equation [59]:

$$\dot{\rho}(t) = i[\rho(t), H'(t)] + \frac{1}{2}\sum_{l=-,z} \Gamma_l \mathcal{L}(\mathcal{A}_l), \tag{16}$$

where $H'(t)$ is the Hamiltonian with systematic errors; $\rho(t)$ is the density matrix of the quantum system; $\mathcal{L}(\mathcal{A}) = 2\mathcal{A}\rho\mathcal{A}^\dagger - \mathcal{A}^\dagger\mathcal{A}\rho - \rho\mathcal{A}^\dagger\mathcal{A}$; $\mathcal{A}_- = |0\rangle\langle 1|$; $\mathcal{A}_z = |1\rangle\langle 1| - |0\rangle\langle 0|$; and Γ_- and Γ_z are the decay and dephasing rates, respectively. We define the gate fidelity as $F = 1/6\sum_{k=1}^{6}\langle\Psi_k(0)|U^\dagger(\tau)\rho(\tau)U(\tau)|\Psi_k(0)\rangle$ [60], with $|\Psi_k(0)\rangle \in \{|0\rangle, |1\rangle, (|0\rangle + |1\rangle)/\sqrt{2}, (|0\rangle - |1\rangle)/\sqrt{2}, (|0\rangle + i|1\rangle)/\sqrt{2}$, and $(|0\rangle - i|1\rangle)/\sqrt{2}\}$ being the initial states. As depicted in Fig. 4, with decoherence rates of $\Gamma_- = \Gamma_z = \Gamma = 10^{-4}\Omega_m$, the overall performance of the ONGQC scheme surpasses that of the NGQC and DY schemes.

D. Comparison with other optimized schemes

The construction of nonadiabatic geometric quantum gates necessitates meeting the cyclic evolution condition and the parallel-transport condition. These geometric conditions are the foundation for the robustness of nonadiabatic geometric quantum gates. Systematic errors can induce defects in these conditions, leading to nonclosed evolution paths and nonzero dynamical phases [48], thus reducing the robustness of geometric quantum gates. Various optimization approaches have been proposed to enhance the robustness of NGQC and NHQC, such as state-independent NGQC [29], optimal control [49–51], and composite pulse techniques [22,52,53]. Although these optimization schemes can improve the robustness of quantum gates, the improvements do not stem from the geometric nature of the gates but rather from the optimization itself, leaving the fundamental issue of geometric condition defects caused by systematic errors unresolved.

In contrast to previous works, the proposed ONGQC scheme offers a general theoretical framework with enhanced robustness for NGQC by preserving fundamental geometric conditions. Next, we compare our scheme (ONGQC) with the state-independent NGQC (SINGQC) scheme in Ref. [29], the robust NHQC (RNHQC) scheme in Ref. [51], and the composite short-path NHQC (CSNHQC) scheme in Ref. [52] to highlight this distinction.

Here, we take the S gate as an example. The Hamiltonian and corresponding parameter settings used in SINGQC, RNHQC, and CSNHQC are detailed in Appendix D. We compare the robustness of the S gate in different schemes against Rabi errors and frequency-shift errors in Figs. 5(a)

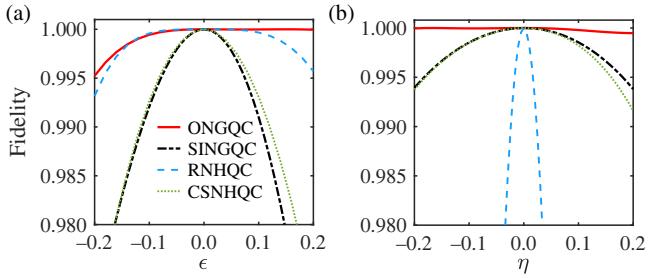

FIG. 5. Robustness of the S gate in different schemes with respect to (a) Rabi error and (b) frequency-shift error.

and 5(b), respectively. We find that the SINGQC, RNHQC, and CSNHQC schemes are robust against either Rabi errors or frequency-shift errors, but not both simultaneously. This work (ONGQC) simultaneously enhances robustness against both types of errors, representing a significant advancement in the field of nonadiabatic geometric quantum computation.

Although the SINGQC, RNHQC, and CSNHQC schemes can enhance the robustness of quantum gates in some cases, this enhancement is not derived from their geometric nature but merely through optimization. As shown in Figs. 6 and 7, after optimization, these schemes either do not satisfy the cyclic condition or have nonzero dynamical phases. Our ONGQC scheme maximizes the preservation of the geometric nature of geometric quantum gates, ensuring both the cyclic evolution and parallel-transport conditions, and thus, guaranteeing the robustness of geometric quantum gates. This significantly enhances the practicality and reliability of geometric quantum gates, paving the way for their implementation in complex quantum computation systems.

III. PHYSICAL IMPLEMENTATION

In this section, we propose to implement our ONGQC scheme on superconducting quantum circuits [61]. Numerical evaluations suggest that high-quality quantum gates can be achieved with state-of-the-art technologies.

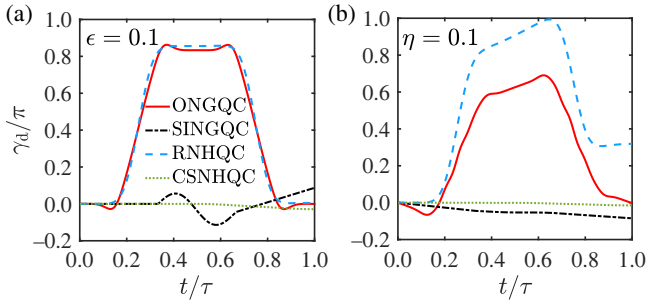

FIG. 6. Dynamic phase $\gamma_d(t)$ in Eq. (12) of the S gate. (a) Rabi error with $\epsilon = 0.1$; (b) frequency-shift error with $\eta = 0.1$. When $\gamma_d(\tau) = 0$, there is no accumulation of dynamical phase.

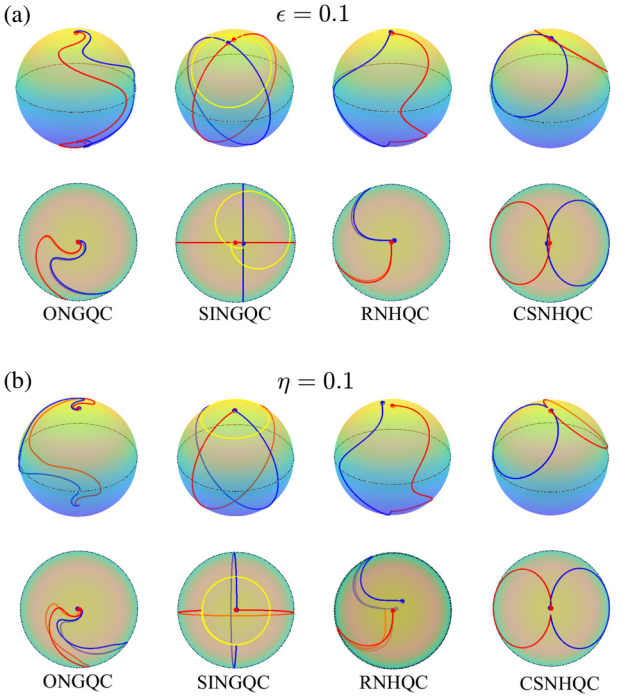

FIG. 7. Evolution paths for the S gate in different schemes are illustrated, (a) considering a Rabi error of $\epsilon = 0.1$, and (b) considering a frequency-shift error of $\eta = 0.1$. Top row displays three-dimensional representations, while the bottom row shows projections onto the X-Y plane. In the evolution-path diagrams, red dots represent the initial states, and blue dots represent the final states. Coincidence of red and blue dots indicates satisfaction of the cyclic condition, while their noncoincidence indicates a failure to satisfy this condition.

A. Single-qubit quantum gates

We consider two-dimensional (2D) superconducting quantum circuits consisting of capacitively coupled transmon qubits [62,63], as depicted in Fig. 8(a). For the construction of single-qubit gates, we focus on the lowest-three energy levels of a transmon qubit, denoted as $\{|0\rangle, |1\rangle, |2\rangle\}$, where $\{|0\rangle, |1\rangle\}$ form the computational space, and $\{|2\rangle\}$ is the main leakage space, as illustrated in Fig. 8(b). We consider that a transmon qubit is driven by an external microwave field, and the system Hamiltonian is given by

$$H_D(t) = (1+\epsilon)\mathbf{A(t)}\cdot\mathbf{S} - \alpha|2\rangle\langle 2| + m\eta\Omega_m \sum_{m=1,2} |m\rangle\langle m|, \tag{17}$$

where α denotes the intrinsic anharmonicity of the transmon; ϵ and η are the Rabi and frequency-shift error ratios, respectively. To mitigate information leakage to noncomputational spaces, we employ "derivative removal via adiabatic gate" (DRAG) technology [64]. The corresponding control field, $\mathbf{A}(t) = \mathbf{A}_0(t) + \mathbf{A}_D(t)$, comprises the original

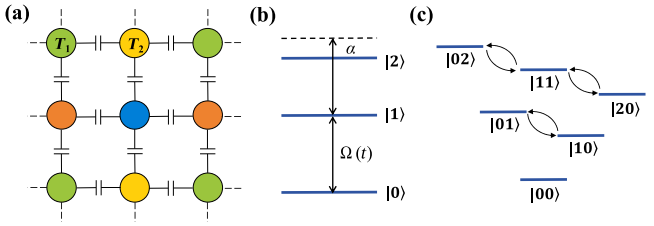

FIG. 8. Illustration of our physical implementation. (a) 2D square superconducting transmon-qubit lattice consists of capacitively coupled transmons. (b) Energy-level diagram of a single driven qubit, where microwave fields are applied to induce the couple of the two lowest levels, but the dispersive transitions among the higher excited states are stimulated because of the weak anharmonicity (α) nature of the transmon qubit. (c) Energy spectrum of two capacitively coupled transmons, where two-excitation subspace can be used to implement the CZ gate.

component, $\mathbf{A}_0(t) = (A_x, A_y, A_z) = (\Omega_R, \Omega_I, 0)$, and the additional DRAG correcting component, $\mathbf{A}_D(t) = (-\dot{A}_y + A_z A_x, \dot{A}_x + A_z A_y, 0)/(-2\alpha)$. The operator vector, $\mathbf{S}$, is specifically written as $S_x = \sum_{m=0,1} \sqrt{m+1}(|m+1\rangle\langle m| + |m\rangle\langle m+1|)$, $S_y = \sum_{m=0,1} \sqrt{m+1}(i|m+1\rangle\langle m| - i|m\rangle\langle m+1|)$, and $S_z = \sum_{m=0,1}(1-2m)|m\rangle\langle m|$.

We assess the performance of quantum gates in a superconducting transmon system, using the S gate as an illustrative example. In this context, the decoherence operators in the master equation are $\mathcal{A}_- = |0\rangle\langle 1| + \sqrt{2}|1\rangle\langle 2|$ and $\mathcal{A}_z = |1\rangle\langle 1| + 2|2\rangle\langle 2|$, with decoherence rates $\Gamma_- = \Gamma_z = 2\pi \times 2$ kHz, and qubit anharmonicity $\alpha = 2\pi \times 220$ MHz. Utilizing the optimized parameters from case 3 in Table I, we depict the comprehensive performance of the S gate against Rabi and frequency-shift errors in Figs. 9(a)–9(c), and compare it with those of conventional NGQC and DY schemes. In our simulations, we set the maximum pulse amplitude for all schemes to $\Omega_m = 2\pi \times 20$ MHz, resulting in gate durations of 90 ns for the ONGQC scheme, 50 ns for the conventional NGQC scheme, and 37.5 ns for the DY scheme. Clearly, in the presence of decoherence, the ONGQC scheme exhibits superior robustness to that of the corresponding NGQC and DY schemes, as shown in Figs. 9(a)–9(c).

B. Two-qubit quantum gates

We now proceed to construct a nontrivial two-qubit geometric gate between two capacitively coupled transmon qubits, denoted as T_1 and T_2, as depicted in Fig. 8(a). The Hamiltonian of two coupled qubits is

$$H_{12}(t) = \sum_{m=1,2}\sum_{j=1,2}[j\,\omega_m - (j-1)\alpha_m]|j\rangle_m\langle j| + g_{12}\prod_{m=1,2}\left(\sum_{j=1,2}\lambda_j\sigma_j^m\right) + \text{H.c.}, \tag{18}$$

where ω_m and α_m are the intrinsic qubit frequency and anharmonicity of T_m, respectively. Additionally, g_{12} is the coupling strength between the two capacitively coupled transmons, $\sigma_j^m = |j\rangle_m\langle j-1|$, $\lambda_1 = 1$, and $\lambda_2 = \sqrt{2}$. Once transition frequencies of adjacent transmon qubits are set, their coupling strength, g_{12}, is generally fixed. To achieve controllable coupling [65,66], we add an ac driving on the transmon qubit, T_1, to adjust its qubit frequency, i.e., $\omega_1(t) = \omega_1 + \dot{F}(t)$, where $F(t) = \beta\sin(\nu t + \phi)$, and ν and ϕ represent the frequency and phase of the driving field, respectively. By utilizing the Jacobi-Anger identity, $\exp[i\beta\cos(\nu t + \phi)] = \sum_{m=-\infty}^{\infty} i^m J_m(\beta)\exp[im(\nu t + \phi)]$, with $J_m(\beta)$ denoting Bessel functions of the first kind, the Hamiltonian in the interaction picture can be expressed as

$$\begin{aligned} H_{12}^I(t) = g_{12}J_1(\beta)e^{-i(\nu t+\phi)}\{&|01\rangle\langle 10|e^{i\Delta t} \\ &+ \sqrt{2}|11\rangle\langle 20|e^{i(\Delta+\alpha_1)t} \\ &+ \sqrt{2}|02\rangle\langle 11|e^{i(\Delta-\alpha_2)t}\} + \text{H.c.}, \end{aligned} \tag{19}$$

where $|kl\rangle = |k\rangle \otimes |l\rangle$, and $\Delta = \omega_1 - \omega_2$ denotes the qubit-frequency difference. The resonant interaction can be induced in the single- or two-excitation subspaces by selecting different driving frequencies, ν, and the corresponding energy-level diagram is shown in Fig. 8(c).

When we set $\Delta - \alpha_2 = \nu$ and neglect high-order oscillating terms, the effectively resonant interaction Hamiltonian in the two-excitation subspace, $\{|02\rangle, |11\rangle\}$, can be written as

$$H_{12}'(t) = \begin{pmatrix} 0 & g_{12}'e^{-i\phi} \\ g_{12}'e^{i\phi} & 0 \end{pmatrix}, \tag{20}$$

where $g_{12}' = \sqrt{2}g_{12}J_1(\beta)$ represents the effective coupling strength, and $J_1(\beta)$ is the first-order Bessel function. Since Eq. (20) has the same form as Eq. (1), state $|11\rangle$ can accumulate a purely geometric phase, similarly to the single-qubit case. Therefore, in the whole two-qubit computational subspace, $\{|00\rangle, |01\rangle, |10\rangle, |11\rangle\}$, we can achieve a two-qubit geometric control-phase gate, i.e.,

$$U'(\tau) = \text{diag}(1, 1, 1, e^{i\gamma'}). \tag{21}$$

For a two-qubit geometric gate, we can also use the optimization strategy to mitigate the influence of systematic errors. Here, the Rabi-error term we consider is $g_{12} \to (1+\epsilon)g_{12}$, and the frequency-shift-error term is $\eta g_{12}(|11\rangle\langle 11| + |22\rangle\langle 22|)$. Here, we take the CZ gate ($\gamma' = \pi$) as an example to assess the performance of our scheme. The optimized parameters are $c_1 = 0.006$, $c_2 = 0.001$, $c_3 = 0.01$, $c_4 = 0.026$, and $c_5 = 0.015$. For a coupling strength of $g_{12} = 2\pi \times 13$ MHz, the optimized gate

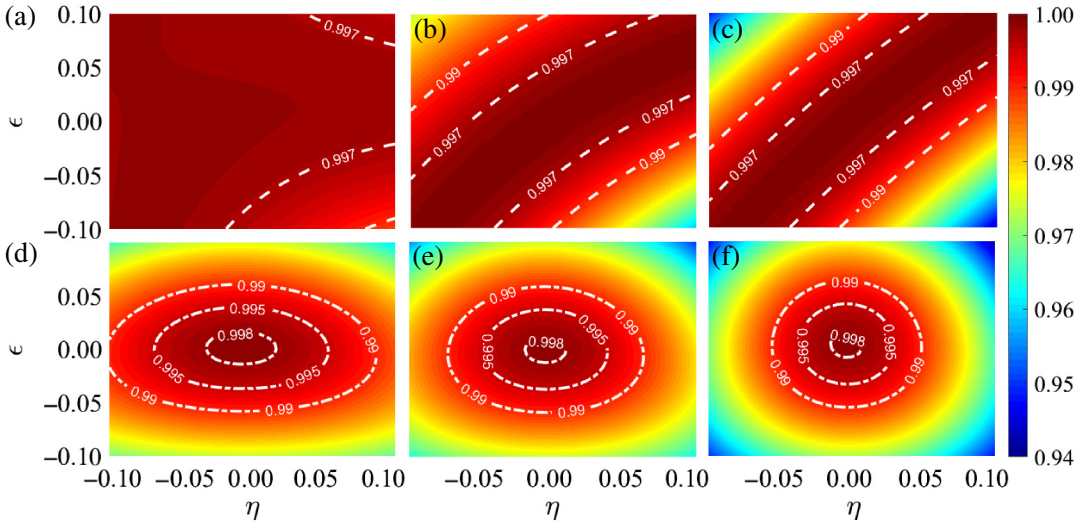

FIG. 9. Robustness of quantum gates against Rabi and frequency-shift errors in superconducting quantum systems. Robustness of the S gate in (a) ONGQC, (b) NGQC, and (c) DY schemes, and CZ gate in (d) ONGQC, (e) NGQC, and (f) DY schemes. Decoherence rate is $\Gamma = 2\pi \times 2$ kHz.

duration is $\tau = 73$ ns. The anharmonicities of transmon qubits are set as $\alpha_1 = 2\pi \times 220$ MHz and $\alpha_2 = 2\pi \times 350$ MHz [61]. To test our gate performance, we define the gate fidelity as $F' = 1/16 \sum_{k=1}^{16} \langle \Psi_k'(0)|U'^{\dagger}(\tau)\rho' U'(\tau)|\Psi_k'(0)\rangle$, where ρ' is the two-atom density operator, and $|\Psi_k'(0)\rangle = |\psi_{k1}'(0)\rangle \otimes |\psi_{k2}'(0)\rangle$ is the initial state of the two qubits, with $|\psi_{kj}'(0)\rangle$ $(j = 1, 2)$ denoting the ith qubit initially in one of the states $\{|0\rangle, |1\rangle, (|0\rangle + |1\rangle)/\sqrt{2}, (|0\rangle - i|1\rangle)/\sqrt{2}\}$ [46]. The decoherence rates of the j qubit are $\Gamma_-^j = \Gamma_z^j = 2\pi \times 2$ kHz. With these settings, the robustness of the ONGQC scheme surpasses that of the NGQC scheme and the DY scheme, achieving the highest fidelity of 99.86%, as depicted in Figs. 9(d)–9(f).

IV. CONCLUSION

We investigate the influence of systematic errors on cyclic evolution and parallel-transport conditions, presenting an ONGQC approach to maximize the preservation of these conditions in the presence of errors. Numerical simulations reveal a substantial boost in gate robustness. The comprehensive performance of geometric single- and two-qubit gates, implemented on superconducting quantum circuits, outperforms those of conventional NGQC and standard DY schemes. This highlights the distinct advantage of the ONGQC scheme in resisting error interference, providing heightened reliability and stability in practical applications. In addition, this extensible approach of the ONGQC scheme can be applied to other physical platforms, such as quantum dots and trapped ions. Therefore, our scheme provides a promising way to achieve large-scale fault-tolerant quantum computation.

ACKNOWLEDGMENTS

This work was supported by the National Natural Science Foundation of China (Grant No. 12275090) and the Starting Research Fund from the Guangxi Normal University (Grant No. DC2300003297).

APPENDIX A: THE CONVENTIONAL NGQC SCHEME

Here, we construct the nonadiabatic geometric gates by using the conventional NGQC scheme [21,22]. In the interaction picture, the Hamiltonian in a resonant two-level system can be written as

$$H_c(t) = \begin{pmatrix} 0 & \Omega_c(t)e^{-i\phi_c} \\ \Omega_c(t)e^{i\phi_c} & 0 \end{pmatrix}, \tag{A1}$$

where $\Omega_c(t) = \Omega_m \sin^2(\pi t/T)$ and ϕ_c denote the strength and phase of the driving field, respectively. The entire evolution time, T, is divided into three parts to obtain a geometric evolution, and the pulse area and relative phase ϕ_c within each segment meet the following conditions:

$$\begin{aligned} &\int_0^{T_1} \Omega_c(t)\mathrm{d}t = \theta_c, \phi_c = \phi - \frac{\pi}{2}, \quad t \in [0, T_1], \\ &\int_{T_1}^{T_2} \Omega_c(t)\mathrm{d}t = \pi, \phi_c = \phi + \gamma + \frac{\pi}{2}, \quad t \in [T_1, T_2], \\ &\int_{T_2}^{T} \Omega_c(t)\mathrm{d}t = \pi - \theta_c, \phi_c = \phi - \frac{\pi}{2}, \quad t \in [T_2, T]. \end{aligned} \tag{A2}$$

The corresponding evolution operator is given by

$$\begin{aligned} U_c(T) &= U_c(T,T_2)U_c(T_2,T_1)U_c(T_1,0), \\ &= \cos\gamma + \sin\gamma \begin{pmatrix} \cos\theta_c & \sin\theta_c e^{-i\phi} \\ \sin\theta_c e^{i\phi} & -\cos\theta_c \end{pmatrix}, \\ &= e^{i\gamma \mathbf{n}\cdot\sigma} \end{aligned} \tag{A3}$$

where $\mathbf{n} = (\sin\theta_c\cos\phi, \sin\theta_c\sin\phi, \cos\theta_c)$ is a unit vector in any direction on the Bloch Sphere, and $\sigma = (\sigma_x, \sigma_y, \sigma_z)$ are the Pauli operators for the computational subspace $\{|0\rangle,\ |1\rangle\}$. Consequently, any single-qubit nonadiabatic geometric gate can be realized by selecting appropriate parameters θ_c, ϕ, and γ. To demonstrate that $U_c(T)$ is an arbitrary single-qubit geometric gate, we take the orthogonal eigenstates of $\mathbf{n}\cdot\sigma$ as

$$\begin{aligned} |\nu_+\rangle &= \cos\frac{\theta_c}{2}|0\rangle + e^{i\phi}\sin\frac{\theta_c}{2}|1\rangle, \\ |\nu_-\rangle &= e^{-i\phi}\sin\frac{\theta_c}{2}|0\rangle - \cos\frac{\theta_c}{2}|1\rangle. \end{aligned} \tag{A4}$$

The evolution operator can be expressed as

$$U_c(T) = e^{i\gamma}|\nu_+\rangle\langle\nu_+| + e^{-i\gamma}|\nu_-\rangle\langle\nu_-|. \tag{A5}$$

Obviously, the orthogonal states $|\nu_\pm\rangle$ satisfy the cyclic evolution condition and the parallel-transport condition in the above evolutionary process, i.e., $|\nu_\pm(T)\rangle = U_c(T)|\nu_\pm\rangle = e^{\pm i\gamma}|\nu_\pm\rangle$ and $\langle\nu_\pm|U_c^\dagger(t)H_c(t)U_c(t)|\nu_\pm\rangle = 0$. Therefore, we can construct any single-qubit gate in a geometric way by selecting appropriate parameters θ_c, ϕ, and γ; here, we choose the S gate and X gate as two typical examples, which correspond to the parameters $\theta_c = 0$, $\phi = 0$, and $\gamma = \pi/4$ and $\theta_c = \pi/2$, $\phi = 0$, and $\gamma = \pi/2$, respectively.

APPENDIX B: THE DYNAMICAL SCHEME

In the dynamical scheme, the Hamiltonian of the system is the same as Eq. (A1), i.e.,

$$H_d(t) = \begin{pmatrix} 0 & \Omega_d(t)e^{-i\phi_d} \\ \Omega_d(t)e^{i\phi_d} & 0 \end{pmatrix}, \tag{B1}$$

where $\Omega_d(t) = \Omega_m\sin^2(\pi t/T)$ and ϕ_d represent the strength and phase of the driving field, respectively. The corresponding evolution operator is given by $U_d(\theta_d,\phi_d) = \cos\theta_d\mathbf{I} - i\sin\theta_d(\cos\phi_d\sigma_x + \sin\phi_d\sigma_y)$, where $\theta_d = \int_0^T \Omega(t)\mathrm{d}t$. By choosing appropriate parameters, the S gate and X gate can be expressed as

$$U_d^S(\theta_d,\phi_d) = U_d\left(\frac{\pi}{4},\pi\right)U_d\left(\frac{\pi}{4},-\frac{3\pi}{2}\right)U_d\left(\frac{\pi}{4},0\right), \tag{B2}$$

$$U_d^X(\theta_d,\phi_d) = U_d(\pi,0). \tag{B3}$$

APPENDIX C: GATE FIDELITY UNDER QUANTUM ERRORS

When considering the influence of systematic errors, the Hamiltonian becomes $H'(t) = H(t) + V(t)$, where the error term $V(t)$ is defined in Eq. (7) in the main text. The evolution operator incorporating errors is then given by $U'(\tau) = \sum_{j=\pm}|\psi_j'(\tau)\rangle\langle\psi_j(0)|$, where $|\psi_j'(\tau)\rangle$ are the evolution states satisfying the Schrödinger equation: $i|\dot{\psi}'(t)\rangle = H'(t)|\psi'(t)\rangle$. The gate fidelity is defined as [58]

$$\begin{aligned} F &= \frac{1}{2}|Tr(U^\dagger(\tau)U'(\tau))|, \\ &= \frac{1}{2}[\langle\psi_+'(\tau)|\psi_+(\tau)\rangle + \langle\psi_-'(\tau)|\psi_-(\tau)\rangle]. \end{aligned} \tag{C1}$$

By using the time-dependent perturbation theory to expand the gate fidelity, we can obtain

$$\langle\psi_+'(\tau)|\psi_+(\tau)\rangle = 1 + \mathcal{O}_1 + \mathcal{O}_2 + \cdots, \tag{C2}$$

where $\mathcal{O}_n$ denotes the error term of total order n. The first two terms are

$$\mathcal{O}_1 = -i\int_0^T e(t)\mathrm{d}t, \tag{C3a}$$

$$\mathcal{O}_2 = -\int_0^T \mathrm{d}t\int_0^t \mathrm{d}t'[e(t)e(t') + g^*(t)g(t')], \tag{C3b}$$

with

$$e = \langle\psi_+|V|\psi_+\rangle = -\frac{1}{2}(\eta\Omega_m\cos\theta - \epsilon\dot{f}\sin^2\theta), \tag{C4a}$$

$$g = \langle\psi_+|V|\psi_-\rangle = \frac{1}{2}\left[\eta\Omega_m\sin\theta + \epsilon\left(\frac{1}{2}\dot{f}\sin 2\theta - i\dot{\theta}\right)\right]e^{if}. \tag{C4b}$$

The other terms can be determined from a symbolic diagram [67,68]. Similarly, we can obtain

$$\begin{aligned} \langle\psi_-'(\tau)|\psi_-(\tau)\rangle = 1 &+ i\int_0^T e(t)\mathrm{d}t \\ &- \int_0^T \mathrm{d}t\int_0^t \mathrm{d}t'[e(t)e(t') + g(t)g^*(t')]. \end{aligned} \tag{C5}$$

Substituting Eqs. (C2) and (C5) into Eq. (C1), and up to the second order, we have

$$\begin{aligned} F &= 1 + \mathcal{O}_2, \\ &= 1 - \frac{1}{2}\left[\int_0^T e(t)\mathrm{d}t\right]^2 - \frac{1}{2}\left[\int_0^T g(t)\mathrm{d}t\right]^2, \end{aligned} \tag{C6}$$

where the property of $\int_0^T \mathrm{d}t\int_0^t \mathrm{d}t'[a(t)b(t') + a(t')b(t)] = \int_0^T a(t)\mathrm{d}t\int_0^T b(t)\mathrm{d}t$ has been used. When considering only

TABLE II. Hamiltonian and corresponding parameter settings adopted in SINGQC, RNHQC, and CSNHQC schemes.

Scheme	Hamiltonian	Pulse shape	Phase
SINGQC Ref. [29]	$H_1(t) = \Omega_1 e^{-i(\frac{\pi}{2}+\varphi_0)}\|0\rangle\langle 1\| + \text{H.c.},$ $H_2(t) = \left[\Omega_2 e^{-i\varphi(t)}\|0\rangle\langle 1\| + \text{H.c.}\right] + \Delta\sigma_z,$ $H_3(t) = \Omega_3 e^{-i[\frac{\pi}{2}+\varphi(\tau_2)]}\|0\rangle\langle 1\| + \text{H.c.},$	$\int_0^{\tau_1}\Omega_1 dt = \frac{2\pi-\theta_1}{2},$ $\Omega_2 = -\frac{1}{2}\sin\theta_1\cos\theta_1\dot{\varphi}(t)$ $\Delta = \frac{1}{2}\sin^2\theta_1\dot{\varphi}(t),$ $\int_{\tau_2}^{\tau_3}\Omega_3 dt = \frac{0-(2\pi-\theta_1)}{2},$	$\varphi_0 = 0,$ $\varphi(t) = \frac{2\pi(t-\tau_1)}{\cos\theta_1(\tau_2-\tau_1)}$ $\varphi(\tau_2) = \frac{2\pi}{\cos\theta_1},$ $\theta_1 = \arccos\frac{\pi}{\gamma+\pi},$ $\gamma = \frac{\pi}{4},$
RNHQC Ref. [51]	$H_r(t) = \Omega_r(t)e^{-i\phi_0(t)}\|b\rangle\langle e\| + \text{H.c.},$	$\Omega_r(t) = \sqrt{\Omega_R^2+\Omega_I^2},$ $\Omega_R = \cos\varphi\sin\chi\dot{f} - \sin\varphi\dot{\chi},$ $\Omega_I = \sin\varphi\sin\chi\dot{f} + \cos\varphi\dot{\chi},$ $\chi = \pi\sin^2[\pi t/T]$ $f = [2\chi - \sin(2\chi)],$	$\dot{\varphi} = -\dot{f}\cos\chi,$ $\int_0^{T/2}\dot{f}\cos\chi\,dt = 0,$ $\int_{T/2}^{T}\dot{f}\cos\chi\,dt = 0,$ $\varphi(0) = -\pi/2,$ $\varphi(T/2) = -\pi,$ $\tan\phi_0 = \Omega_I/\Omega_R,$
CSNHQC Ref. [52]	$H_c(t) = \left\{\Omega_c(t)e^{-i[\beta(t)+\chi(t)]}\|b\rangle\langle e\| + \text{H.c.}\right\}$ $+\Delta(t)\|e\rangle\langle e\|$	$\Omega_c(t) = \sqrt{[\dot{\beta}\sin\alpha]^2+\dot{\alpha}^2}/2$ $\triangle(t) = -\dot{\beta}(t)\,[1+\cos\alpha(t)]$	$\beta = \beta_0 + \pi\sin^2(\pi t/2/T),$ $\alpha = 2\arctan[l\sin\beta - \beta_0],$ $l = \sqrt{2\pi\gamma-\gamma^2}/(\pi-\gamma),$ $\chi = \arctan\{\dot{\alpha}/[\dot{\beta}\sin\alpha]\},$ $\beta_0 = 0, t\in[0,T],$ $\beta_0 = \pi, t\in[T,2T],$ $\gamma = \pi/4,$

the frequency-shift error, the gate fidelity becomes $F_\eta = 1-\mathcal{E}^\eta$, where

$$\mathcal{E}^\eta = \frac{1}{8}\left(\left|\int_0^\tau \eta\Omega_m\cos\theta\,dt\right|^2 + \left|\int_0^\tau \eta\Omega_m\sin\theta e^{if}\,dt\right|^2\right), \tag{C7}$$

and when considering only the Rabi error, the gate fidelity becomes $F_\epsilon = 1-\mathcal{E}^\epsilon$, with

$$\mathcal{E}^\epsilon = \frac{1}{8}\left(\left|\int_0^\tau \epsilon\dot{f}\sin^2\theta\,dt\right|^2 + \left|\int_0^\tau \epsilon(\frac{1}{2}\dot{f}\sin 2\theta - i\dot{\theta})e^{if}\,dt\right|^2\right). \tag{C8}$$

Considering both the Rabi and frequency-shift error, the gate fidelity can be written as

$$F = 1-\mathcal{E}^\epsilon - \mathcal{E}^\eta. \tag{C9}$$

APPENDIX D: THE CONSTRUCTION OF OTHER OPTIMIZATION CONTROLS

We now briefly introduce the optimization schemes presented in Refs. [29,51,52], which correspond to the SINGQC, RNHQC, and CSNHQC schemes, respectively. The Hamiltonians and corresponding parameter settings used in these proposals are summarized in Table II. The SINGQC scheme employs a simple two-level structure, while the RNHQC and CSNHQC schemes require a three-level quantum system composed of two low-energy states, $|0\rangle$ and $|1\rangle$, along with an auxiliary excited state, $|e\rangle$, as they construct nonadiabatic holonomic quantum gates. In the Hamiltonians $H_r(t)$ and $H_c(t)$, the state $|b\rangle$ represents the bright state [51,52].

Figure 5(a) in the main text shows the robustness of the S gate in different schemes against Rabi-frequency errors $[\Omega\to(1+\epsilon)\Omega]$, and Fig. 5(b) in the main text demonstrates the robustness of the S gate in different schemes against the frequency-shift error. The form of the frequency-shift error in the SINGQC scheme is $\eta\Omega_m\sigma_z$, while in the RNHQC and CSNHQC schemes, it is

$\eta\Omega_m|e\rangle\langle e|$. Here, Ω denotes the Rabi frequency, Ω_m represents the maximum value of Rabi frequency Ω, σ_z denotes the Pauli-Z operator, and ϵ and η denote error ratios.

[1] P. W. Shor, Polynomial-time algorithms for prime factorization and discrete logarithms on a quantum computer, SIAM J. Comput. **26**, 1484 (1997).

[2] M. V. Berry, Quantal phase factors accompanying adiabatic changes, Proc. R. Soc. Lond. A **392**, 45 (1984).

[3] Y. Aharonov and J. Anandan, Phase change during a cyclic quantum evolution, Phys. Rev. Lett. **58**, 1593 (1987).

[4] F. Wilczek and A. Zee, Appearance of gauge structure in simple dynamical systems, Phys. Rev. Lett. **52**, 2111 (1984).

[5] J. Anandan, Non-adiabatic non-abelian geometric phase, Phys. Lett. A **133**, 171 (1988).

[6] S.-L. Zhu and P. Zanardi, Geometric quantum gates that are robust against stochastic control errors, Phys. Rev. A **72**, 020301(R) (2005).

[7] P. Solinas, M. Sassetti, P. Truini, and N. Zanghì, On the stability of quantum holonomic gates, New J. Phys. **14**, 093006 (2012).

[8] M. Johansson, E. Sjöqvist, L. M. Andersson, M. Ericsson, B. Hessmo, K. Singh, and D. M. Tong, Robustness of nonadiabatic holonomic gates, Phys. Rev. A **86**, 062322 (2012).

[9] J. A. Jones, V. Vedral, A. Ekert, and G. Castagnoli, Geometric quantum computation using nuclear magnetic resonance, Nature (London) **403**, 869 (2000).

[10] L.-M. Duan, J. I. Cirac, and P. Zoller, Geometric manipulation of trapped ions for quantum computation, Science **292**, 1695 (2001).

[11] X.-B. Wang and M. Keiji, Nonadiabatic conditional geometric phase shift with NMR, Phys. Rev. Lett. **87**, 097901 (2001).

[12] S.-L. Zhu and Z. D. Wang, Implementation of universal quantum gates based on nonadiabatic geometric phases, Phys. Rev. Lett. **89**, 097902 (2002).

[13] E. Sjöqvist, D.-M. Tong, L. M. Andersson, B. Hessmo, M. Johansson, and K. Singh, Non-adiabatic holonomic quantum computation, New J. Phys. **14**, 103035 (2012).

[14] G.-F. Xu, J. Zhang, D.-M. Tong, E. Sjöqvist, and L. C. Kwek, Nonadiabatic holonomic quantum computation in decoherence-free subspaces, Phys. Rev. Lett. **109**, 170501 (2012).

[15] Y.-X. Du, Z.-T. Liang, H. Yan, and S.-L. Zhu, Geometric quantum computation with shortcuts to adiabaticity, Adv. Quantum Technol. **2**, 1900013 (2019).

[16] J. Zhang, T. H. Kyaw, S. Filipp, L.-C. Kwek, E. Sjöqvist, and D.-M. Tong, Geometric and holonomic quantum computation, Phys. Rep. **1027**, 1 (2023).

[17] Y. Liang, P. Shen, T. Chen, and Z.-Y. Xue, Nonadiabatic holonomic quantum computation and its optimal control, Sci. China Inf. Sci. **66**, 180502 (2023).

[18] S.-L. Zhu and Z.-D. Wang, Unconventional geometric quantum computation, Phys. Rev. Lett. **91**, 187902 (2003).

[19] X.-D. Zhang, S.-L. Zhu, L. Hu, and Z.-D. Wang, Nonadiabatic geometric quantum computation using a single-loop scenario, Phys. Rev. A **71**, 014302 (2005).

[20] S.-L. Zhu, C. Monroe, and L.-M. Duan, Trapped ion quantum computation with transverse phonon modes, Phys. Rev. Lett. **97**, 050505 (2006).

[21] P.-Z. Zhao, X.-D. Cui, G.-F. Xu, E. Sjöqvist, and D.-M. Tong, Rydberg-atom-based scheme of nonadiabatic geometric quantum computation, Phys. Rev. A **96**, 052316 (2017).

[22] T. Chen and Z.-Y. Xue, Nonadiabatic geometric quantum computation with parametrically tunable coupling, Phys. Rev. Appl. **10**, 054051 (2018).

[23] B.-J. Liu, S.-L. Su, and M.-H. Yung, Nonadiabatic noncyclic geometric quantum computation in Rydberg atoms, Phys. Rev. Res. **2**, 043130 (2020).

[24] K.-Z. Li, P.-Z. Zhao, and D.-M. Tong, Approach to realizing nonadiabatic geometric gates with prescribed evolution paths, Phys. Rev. Res. **2**, 023295 (2020).

[25] T. Chen and Z.-Y. Xue, High-fidelity and robust geometric quantum gates that outperform dynamical ones, Phys. Rev. Appl. **14**, 064009 (2020).

[26] L.-N. Ji, C.-Y. Ding, T. Chen, and Z.-Y. Xue, Noncyclic geometric quantum gates with smooth paths via invariant-based shortcuts, Adv. Quantum Technol. **4**, 2100019 (2021).

[27] C.-Y. Ding, Y. Liang, K.-Z. Yu, and Z.-Y. Xue, Nonadiabatic geometric quantum computation with shortened path on superconducting circuits, Appl. Phys. Lett. **119**, 184001 (2021).

[28] C.-Y. Ding, L.-N. Ji, T. Chen, and Z.-Y. Xue, Path-optimized nonadiabatic geometric quantum computation on superconducting qubits, Quantum Sci. Technol. **7**, 015012 (2021).

[29] Y. Liang, P. Shen, L.-N. Ji, and Z.-Y. Xue, State independent nonadiabatic geometric quantum gates, Phys. Rev. Appl. **19**, 024051 (2023).

[30] G.-F. Xu, C.-L. Liu, P.-Z. Zhao, and D.-M. Tong, Nonadiabatic holonomic gates realized by a single-shot implementation, Phys. Rev. A **92**, 052302 (2015).

[31] E. Herterich and E. Sjöqvist, Single-loop multiple-pulse nonadiabatic holonomic quantum gates, Phys. Rev. A **94**, 052310 (2016).

[32] B.-J. Liu, X.-K. Song, Z.-Y. Xue, X. Wang, and M.-H. Yung, Plug-and-play approach to nonadiabatic geometric quantum gates, Phys. Rev. Lett. **123**, 100501 (2019).

[33] P.-Z. Zhao, K.-Z. Li, G.-F. Xu, and D.-M. Tong, General approach for constructing Hamiltonians for nonadiabatic holonomic quantum computation, Phys. Rev. A **101**, 062306 (2020).

[34] J.-L. Wu, Y. Wang, J.-X. Han, Y. Jiang, J. Song, Y. Xia, S.-L. Su, and W. Li, Systematic-error-tolerant multiqubit holonomic entangling gates, Phys. Rev. Appl. **16**, 064031 (2021).

[35] S.-L. Su, Li-Na Sun, B.-J. Liu, L.-L. Yan, M.-H. Yung, W. Li, and M. Feng, Rabi- and blockade-error-resilient all-geometric Rydberg quantum gates, Phys. Rev. Appl. **19**, 044007 (2023).

[36] D. Leibfried, B. DeMarco, V. Meyer, D. Lucas, M. Barrett, J. Britton, W. M. Itano, B. Jelenković, C. Langer, T. Rosen-

band, and D. J. Wineland, Experimental demonstration of a robust, high-fidelity geometric two ion-qubit phase gate, Nature (London) **422**, 412 (2003).

[37] J. Du, P. Zou, and Z. D. Wang, Experimental implementation of high-fidelity unconventional geometric quantum gates using an NMR interferometer, Phys. Rev. A **74**, 020302(R) (2006).

[38] G.-R. Feng, G.-F. Xu, and G.-L. Long, Experimental realization of nonadiabatic holonomic quantum computation, Phys. Rev. Lett. **110**, 190501 (2013).

[39] A. A. Abdumalikov Jr, J. M. Fink, K. Juliusson, M. Pechal, S. Berger, A. Wallraff, and S. Filipp, Experimental realization of non-abelian non-adiabatic geometric gates, Nature **496**, 482 (2013).

[40] S. Arroyo-Camejo, A. Lazariev, S. W. Hell, and G. Balasubramanian, Room temperature high-fidelity holonomic single-qubit gate on a solid-state spin, Nat. Commun. **5**, 4870 (2014).

[41] C. Zu, W.-B. Wang, L. He, W.-G. Zhang, C.-Y. Dai, F. Wang, and L.-M. Duan, Experimental realization of universal geometric quantum gates with solid-state spins, Nature **514**, 72 (2014).

[42] Y. Sekiguchi, N. Niikura, R. Kuroiwa, H. Kano, and H. Kosaka, Optical holonomic single quantum gates with a geometric spin under a zero field, Nat. Photonics **11**, 309 (2017).

[43] B.-B. Zhou, P. C. Jerger, V. O. Shkolnikov, F. J. Heremans, G. Burkard, and D. D. Awschalom, Holonomic quantum control by coherent optical excitation in diamond, Phys. Rev. Lett. **119**, 140503 (2017).

[44] K. Nagata, K. Kuramitani, Y. Sekiguchi, and H. Kosaka, Universal holonomic quantum gates over geometric spin qubits with polarised microwaves, Nat. Commun. **9**, 3227 (2018).

[45] N. Ishida, T. Nakamura, T. Tanaka, S. Mishima, H. Kano, R. Kuroiwa, Y. Sekiguchi, and H. Kosaka, Universal holonomic single quantum gates over a geometric spin with phase-modulated polarized light, Opt. Lett. **43**, 2380 (2018).

[46] Y. Xu, Z. Hua, T. Chen, X. Pan, X. Li, J. Han, W. Cai, Y. Ma, H. Wang, Y. Song, Z.-Y. Xue, and L. Sun, Experimental implementation of universal nonadiabatic geometric quantum gates in a superconducting circuit, Phys. Rev. Lett. **124**, 230503 (2020).

[47] P.-Z. Zhao, Z. Dong, Z.-X. Zhang, G.-P. Guo, D.-M. Tong, and Y. Yin, Experimental realization of nonadiabatic geometric gates with a superconducting Xmon qubit, Sci. China-Phys. Mech. Astron. **64**, 250362 (2021).

[48] J. T. Thomas, M. Lababidi, and M. Tian, Robustness of single-qubit geometric gate against systematic error, Phys. Rev. A **84**, 042335 (2011).

[49] S. Li, T. Chen, and Z.-Y. Xue, Fast holonomic quantum computation on superconducting circuits with optimal control, Adv. Quantum Technol. **3**, 2000001 (2020).

[50] J. Xu, S. Li, T Chen, and Z.-Y. Xue, Nonadiabatic geometric quantum computation with optimal control on superconducting circuits, Front. Phys. **15**, 41503 (2020).

[51] M.-Z. Ai, S. Li, Z.-B. Hou, R. He, Z.-H. Qian, Z.-Y. Xue, J.-M. Cui, Y.-F. Huang, C.-F. Li, and G.-C. Guo, Experimental realization of nonadiabatic holonomic single-qubit quantum gates with optimal control in a trapped ion, Phys. Rev. Appl. **14**, 054062 (2020).

[52] Y. Liang, P. Shen, T. Chen, and Z.-Y. Xue, Composite short-path nonadiabatic holonomic quantum gates, Phys. Rev. Appl. **17**, 034015 (2022).

[53] Z.-Z. Zhu, T. Chen, X.-D. Yang, J. Bian, Z.-Y. Xue, and X.-H. Peng, Single-loop and composite-loop realization of nonadiabatic holonomic quantum gates in a decoherence-free subspace, Phys. Rev. Appl. **12**, 024024 (2019).

[54] F.-H. Zhang, J. Zhang, P. Gao, and G.-L. Long, Searching nonadiabatic holonomic quantum gates via an optimization algorithm, Phys. Rev. A **100**, 012329 (2019).

[55] D. Guéry-Odelin, A. Ruschhaupt, A. Kiely, E. Torrontegui, S. Martínez-Garaot, and J. G. Muga, Shortcuts to adiabaticity: Concepts, methods, and applications, Rev. Mod. Phys. **91**, 045001 (2019).

[56] Y.-H. Kang, Y.-H. Chen, Q.-C. Wu, B.-H. Huang, Y. Xia, and J. Song, Reverse engineering of a Hamiltonian by designing the evolution operators, Sci. Rep. **6**, 30151 (2016).

[57] J. Zhang, T. H. Kyaw, D.-M. Tong, E. Sjöqvist, and L. C. Kwek, Fast non-abelian geometric gates via transitionless quantum driving, Sci. Rep. **5**, 18414 (2016).

[58] X. G. Wang, Z. Sun, and Z. D. Wang, Operator fidelity susceptibility: An indicator of quantum criticality, Phys. Rev. A **79**, 012105 (2009).

[59] G. Lindblad, On the generators of quantum dynamical semigroups, Commun. Math. Phys. **48**, 119 (1976).

[60] A. Klappenecker and M. Rotteler, Mutually unbiased bases are complex projective 2-designs, Proc. Int. Symp. Inf. Theory **2005**, 1740 (2005).

[61] A. Blais, A. L. Grimsmo, S. M. Girvin, and A. Wallraff, Circuit quantum electrodynamics, Rev. Mod. Phys. **93**, 025005 (2021).

[62] J. Koch, T. M. Yu, J. Gambetta, A. A. Houck, D. I. Schuster, J. Majer, A. Blais, M. H. Devoret, S. M. Girvin, and R. J. Schoelkopf, Charge-insensitive qubit design derived from the Cooper pair box, Phys. Rev. A **76**, 042319 (2007).

[63] J. Q. You, X. Hu, S. Ashhab, and F. Nori, Low-decoherence flux qubit, Phys. Rev. B **75**, 140515(R) (2007).

[64] F. Motzoi, J. M. Gambetta, P. Rebentrost, and F. K. Wilhelm, Simple pulses for elimination of leakage in weakly nonlinear qubits, Phys. Rev. Lett. **103**, 110501 (2009).

[65] X. Li, Y. Ma, J. Han, T. Chen, Y. Xu, W. Cai, H. Wang, Y. P. Song, Z. Y. Xue, Z. Q. Yin, and L. Sun, Perfect quantum state transfer in a superconducting qubit chain with parametrically tunable couplings, Phys. Rev. Appl. **10**, 054009 (2018).

[66] J. Chu, D. Li, X. Yang, S. Song, Z. Han, Z. Yang, Y. Dong, W. Zheng, Z. Wang, X. Yu, D. Lan, X. Tan, and Y. Yu, Realization of superadiabatic two-qubit gates using parametric modulation in superconducting circuits, Phys. Rev. Appl. **13**, 064012 (2020).

[67] D. Daems, A. Ruschhaupt, D. Sugny, and S. Guérin, Robust quantum control by a single-shot shaped pulse, Phys. Rev. Lett. **111**, 050404 (2013).

[68] G. Dridi, K. Liu, and S. Guérin, Optimal robust quantum control by inverse geometric optimization, Phys. Rev. Lett. **125**, 250403 (2020).